Hindawi
Advances in Condensed Matter Physics
Volume 2021, Article ID 4346979, 9 pages
https://doi.org/10.1155/2021/4346979

Research Article

First-Principles Calculation of Conductivity of Ce-C Codoped SnO_2 Contacts

Can Ding,[1] **Zhenjiang Gao**,[1] **Xing Hu**,[1] **and Zhao Yuan**[2]

[1]*College of Electrical Engineering & New Energy, China Three Gorges University, Yichang 443002, China*
[2]*State Key Laboratory of Advanced Electromagnetic Engineering & Technology, Huazhong University of Science and Technology, Wuhan 430074, China*

Correspondence should be addressed to Zhenjiang Gao; 848327159@qq.com

Received 18 July 2021; Revised 16 October 2021; Accepted 5 November 2021; Published 22 November 2021

Academic Editor: Golam M. Bhuiyan

The contact is the core element of the vacuum interrupter of the mechanical DC circuit breaker. The electrical conductivity and welding resistance of the material directly affect its stability and reliability. $AgSnO_2$ contact material has low resistivity, welding resistance, and so on. This material occupies an important position of the circuit breaker contact material. This research is based on the first-principles analysis method of density functional theory. The article calculated the lattice constant, enthalpy change, energy band, electronic density of state, charge density distribution, population, and conductivity of Ce, C single-doped, and Ce-C codoped SnO_2 systems. The results show that Ce, C single doping, and Ce-C codoping all increase the cell volume and lattice constant. When the elements are codoped, the enthalpy change is the largest, and the thermal stability is the best. It has the smallest bandgap, the most impurity energy levels, and the least energy required for electronic transitions. The 4f orbital electrons of the Ce atom and the 2p orbital electrons of C are the sources of impurity energy near the Fermi level. When the elements are codoped, more impurity energy levels are generated at the bottom of the conduction band and the top of the valence band. Its bandgap is reduced so conductivity is improved. From the charge density and population analysis, the number of free electrons of Ce atoms and C atoms is redistributed after codoping. It forms a Ce-C covalent bond to further increase the degree of commonality of electrons and enhance the metallicity. The conductivity analysis shows that both single-doped and codoped conductivity have been improved. When the elements are codoped, the conductivity is the largest, and the conductivity is the best.

1. Introduction

Mechanical DC circuit breakers are important electrical equipment of the power grid. The contact is the core element of the vacuum interrupter of the mechanical DC circuit breaker. It plays the role of connecting, carrying, and breaking current. The electrical conductivity, thermal conductivity, resistance to welding, and arc erosion of the contact material directly affect the stability and reliability of the circuit breaker's arc chamber. It directly affects its stability and reliability. The current ablation resistance of the contacts of the interrupter is still insufficient. After a few breaks, the contacts will appear spotted and cracked. This makes the contact resistance increase, and the conductivity deteriorates, which makes the contacts prone to fusion welding [1–3]. In the subsequent breaking process, the contact gap is prone to produce a large amount of metal vapor. This causes the gap to reignite and cause breaking failure, so the contact life will be greatly reduced. There is an urgent need to improve its electrical conductivity and ablation resistance. The contact material is an important factor influencing changes in its performance. Its optimal selection and design is an extremely important part of mechanical DC circuit breaker design [4–8].

Silver oxide has the advantages of good electrical conductivity, welding resistance, and low contact resistance. Therefore, it is widely used as a contact material. In 1939, Hensel and other scholars developed AgCdO electrical contact material [9–11]. It is also called a universal contact because of its good arc extinguishing, electrical corrosion resistance, and low contact resistance. However, it will

release toxic vapor Cd during use. So it was later replaced by $AgSnO_2$ material. Because the material has the advantages of low electrical resistivity, excellent wear resistance, and welding resistance, thus occupying an important position of the circuit breaker contact material. The material is mainly composed of Ag, and SnO_2 is the doped material. It can prevent the liquid from splashing after the silver melts and enhance the viscosity of the silver. SnO_2 is a wide bandgap semiconductor material; the bandgap is about 3.6 eV; and the exciton bound energy is 130 meV. The conductivity of the material can be improved by doping elements. China has huge reserves of rare earth metals. In recent years, many scholars have doped SnO_2 with rare earth elements, metal elements, and nonmetal elements and have made great progress in improving electrical and mechanical properties [12–22].

Zhao et al. [23] conducted a first-principles analysis on the conductivity of La-doped SnO_2. The study found that the conductivity is the best when the La doping ratio is 16.67%. Li et al. [24] performed first-principles calculations on N-S codoped SnO_2. It was found that when N-S codoped, the orbital cohybridization makes the electrical performance better. Du et al. [25] studied the mechanical properties and electronic structure of different SnO_2 crystals. It is found that the formation of P_{nam} type SnO_2 is relatively difficult. The Vickers hardness values of P_{bca} and P_{nam} type SnO_2 are not significantly different. There are differences in the bandgaps of different crystal structures. The P_{nam} structure has the most obvious absorption of ultraviolet light. Xie et al. [26] studied the electronic structure of Ru-doped SnO_2 solid solution. It is found that as the Ru doping ratio increases. The reduction of the lattice parameters and the forbidden band leads to an increase in the conductivity of the solid solution.

There are both experimental and theoretical [27, 28] studies on Ce single-doped and C-doped SnO_2. However, the theoretical analysis of the electrical properties of Ce-C codoped $AgSnO_2$ contact materials has not been reported yet. Reference [10] calculated that the optimal ratio of La and W codoped with SnO_2 was 16.67%. Reference [23] calculated the best conductivity when the ratio of La-doped SnO_2 was 16.67%. Reference [24] calculated that the optimal ratio of N and S codoped SnO_2 was 16.67%. Reference [27] calculated that the optimal ratio of Ce and Nd codoped with SnO_2 was 16.67%. If the doping concentration is changed, the performance will not be optimal. Because of previous research on SnO_2, this article uses the first-principles method. The relevant parameters when the ratio of Ce and C single doping and codoping is 16.67% are calculated and compared. These parameters include the material's unit cell parameters, enthalpy change, band structure, density of states, charge density distribution, population analysis, and conductivity. The electrical properties of $AgSnO_2$ contacts are analyzed from the first principle of the matter. The study compared the conductivity of Ce, C single-doped, and Ce-C codoped SnO_2 materials. It provides an idea for improving the conductivity of the $AgSnO_2$ contact material in the vacuum interrupter of the DC circuit breaker.

2. Unit Cell Model and Calculation Method

2.1. Unit Cell Model. The ideal SnO_2 has a rutile phase structure with a space group of 136P4/MNM, which belongs to the body-centered tetragonal system. Each initial SnO_2 cell contains 2 Sn atoms and 4 O atoms. This paper uses molecular modeling software to establish a $1 \times 2 \times 3$ SnO_2 supercell model. The established supercell contains 12 Sn atoms and 24 O atoms. This paper studies the effect of rare earth element Ce and nonmetal C-doped SnO_2 on the conductivity of SnO_2. The doping model is established by the method of atom substitution. The nonmetallic O atoms in the supercell is replaced with 4 C atoms. The metal site Sn is replaced with 2 Ce atoms. When the elements are codoped, 2 C and 1 Ce are used instead. The ratios of Ce single doping, C single doping, and Ce-C codoping are all 16.67%. The specific positions of single doping and codoping are shown in Figure 1. The type of atom has been marked in the figure.

2.2. Calculation Method. The research of this thesis uses CASTEP (Cambridge Sequential Total Energy Package) software to calculate. In k-space, the first-principles plane wave supersoft pseudopotential is used to describe the interaction between real ions and valence electrons. The cut-off energy of the plane wave in the inverted lattice space is set to 500 eV. Periodic boundary conditions based on discrete Fourier transform are used. Since the generalized gradient approximation considers the influence of the charge density near a certain position on the exchange-related energy, the exponential charge density region can be appropriately corrected. The calculation adopts the form of generalized gradient approximation GGA + U. The U values applied to the p and d orbits of Sn are 9.6 eV and 3.5 eV, respectively. The U value applied to the 2s and 2p orbitals of O is 9.6 eV. These U values of Sn and O atoms are obtained through collisions and experimental rules. The correction function uses PBE to deal with the exchange correlation energy of the electron-electron interaction. The ground state electrons involved in the calculation are Sn atom 5s2 and 5p2, O atom 2s2 and 2p4, Ce atom 4f1, 5p6, 5d1, and 6s2, and C atom 2s2 and 2p2. The paper uses the BFGS optimization algorithm to optimize the unit cell structure. The convergence criteria are as follows: The total energy convergence value of the system is 2.0×10^{-6} eV/atom. The maximum atomic displacement is 0.002 Å. The interaction force between atoms is 0.05 eV/Å. The internal stress deviation of the crystal is 0.1 GPa. The energy of a single atom is 2×10^{-5} eV/atom. Brillouin zone points are in the form of Monkhorst-Pack. The K point is set to $4 \times 4 \times 6$. The system also optimizes the structure of the computing system.

3. Results and Analysis

3.1. Lattice Constant and Enthalpy Change Value. The supercell parameters after geometric optimization are shown in Table 1. It can be seen that the optimized lattice constants of the intrinsic SnO_2 are $a = b = 4.715$ Å and $c = 3.162$ Å (experimental values $a = b = 4.737$ Å and $c = 3.186$ Å). The

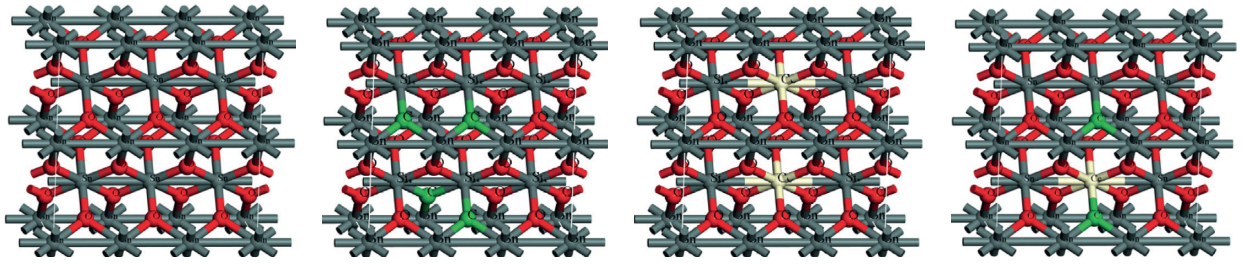

(a) (b) (c) (d)

Figure 1: Supercell models: (a) SnO_2, (b) C-doped, (c) Ce-doped, and (d) Ce-C codoped.

Table 1: Lattice constants, cell volumes, and enthalpy change of SnO_2 before and after doping.

Data resource	a (Å)	b (Å)	c (Å)	Cell volume (Å^3)	Enthalpy change (eV)
This work SnO_2	4.715	4.715	3.162	70.2951	−0.3788
Experiment [29]	4.737	4.737	3.186	71.4912	—
Theory [26]	4.735	4.735	3.188	71.4757	−0.014
This work C-SnO_2	4.894	4.894	3.272	78.3684	−0.4246
Experiment [28]	4.889	4.889	3.321	79.4235	—
Theory [28]	4.885	4.885	3.279	78.2475	—
This work Ce-SnO_2	4.946	4.946	3.389	82.9048	−1.7248
Experiment [30]	4.937	4.937	3.436	83.7489	—
Theory [27]	4.958	4.958	3.346	82.2506	−3.340
This work Ce-C-SnO_2	4.938	4.938	3.381	82.4418	−2.1465

calculation error is very small (about 0.4%). The optimized lattice constants when C doping and Ce-C codoping are basically consistent with other references and experimental values. The error is less than 1.5%. It shows that the calculation method of this research is reasonable, so the next calculation can be carried out. The difference in results is due to the use of different approximation algorithms. But it does not affect the analysis of the results. The lattice constant after doping increases to the intrinsic SnO_2 to varying degrees, and the cell volume also increases. The atomic radius of Ce (1.82 Å) is larger than that of Sn (1.58 Å). The atomic radius of C (8.6 Å) is larger than that of O (6.6 Å). Therefore, according to quantum chemistry theory, it can be known that the rare earth element Ce replaces the Sn site. It will affect the surrounding O atoms. The unit cell forms a Ce-O bond that is longer than the Sn-O bond. When C replaces the O element, a longer Sn-C bond is formed. Therefore, the lattice constant and unit cell volume are increased to different degrees when Ce and C are single-doped. However, the lattice constant and unit cell volume are slightly reduced when Ce and C are codoped than when Ce is single-doped. This is because Ce and C form stronger and shorter bonds in the crystal. This changes the original sequence of atoms in the intrinsic SnO_2 unit cell and causes distortion of the crystal lattice.

This paper also calculates the enthalpy change value (ΔH/eV) of each optimized system. The calculation formula is as follows:

$$\Delta H = H_{\text{End}} - H_{\text{Ini}}, \quad (1)$$

where H_{End} is the system energy that is finally optimized. H_{Ini} is the energy of the original system. The enthalpy change value is an important parameter of the difficulty of formation of the doped structure and the thermodynamic stability. The smaller the value of enthalpy change, the larger the absolute value. The smaller the value of enthalpy change, the more stable the substance is in thermodynamic properties. According to the data in Table 1, the single doping of C and Ce is more stable than the initial state of SnO_2. The enthalpy change value is the smallest when Ce-C codoping. Therefore, its thermodynamic stability is the best.

3.2. Band Structure. The band structure diagram of the initial state SnO_2, Ce C single doping, and Ce-C codoping is shown in Figure 2. The energy band range of −5~15 eV is selected in this study. The energy zero point is the Fermi level. Figure 2(a) is the band diagram of the initial state SnO_2. Its bandgap is 3.553 eV. It is close to the experimental value of 3.6 eV [23] measured in the excited state. It can be seen from the energy band diagram that both the top of the valence band and the bottom of the conduction band are at the high symmetry point G in the Brillouin zone. It can be determined that SnO_2 is a direct bandgap semiconductor material. The energy band near the Fermi level is sparse. Electrons need at least 3.553 eV of energy to travel from the valence band to the conduction band.

The band structures of Ce, C single doping, and Ce-C codoping are shown in Figures 2(b)–2(d). It can be seen that in the energy band diagrams of Figures 2(c) and 2(d), the top of the valence band and the bottom of the conduction band are both at the high symmetry point G in the Brillouin zone. It shows that it is still a direct bandgap semiconductor after doping. Figure 2(b) is the energy band diagram of C-doped SnO_2. The top of the valence band and the bottom of the

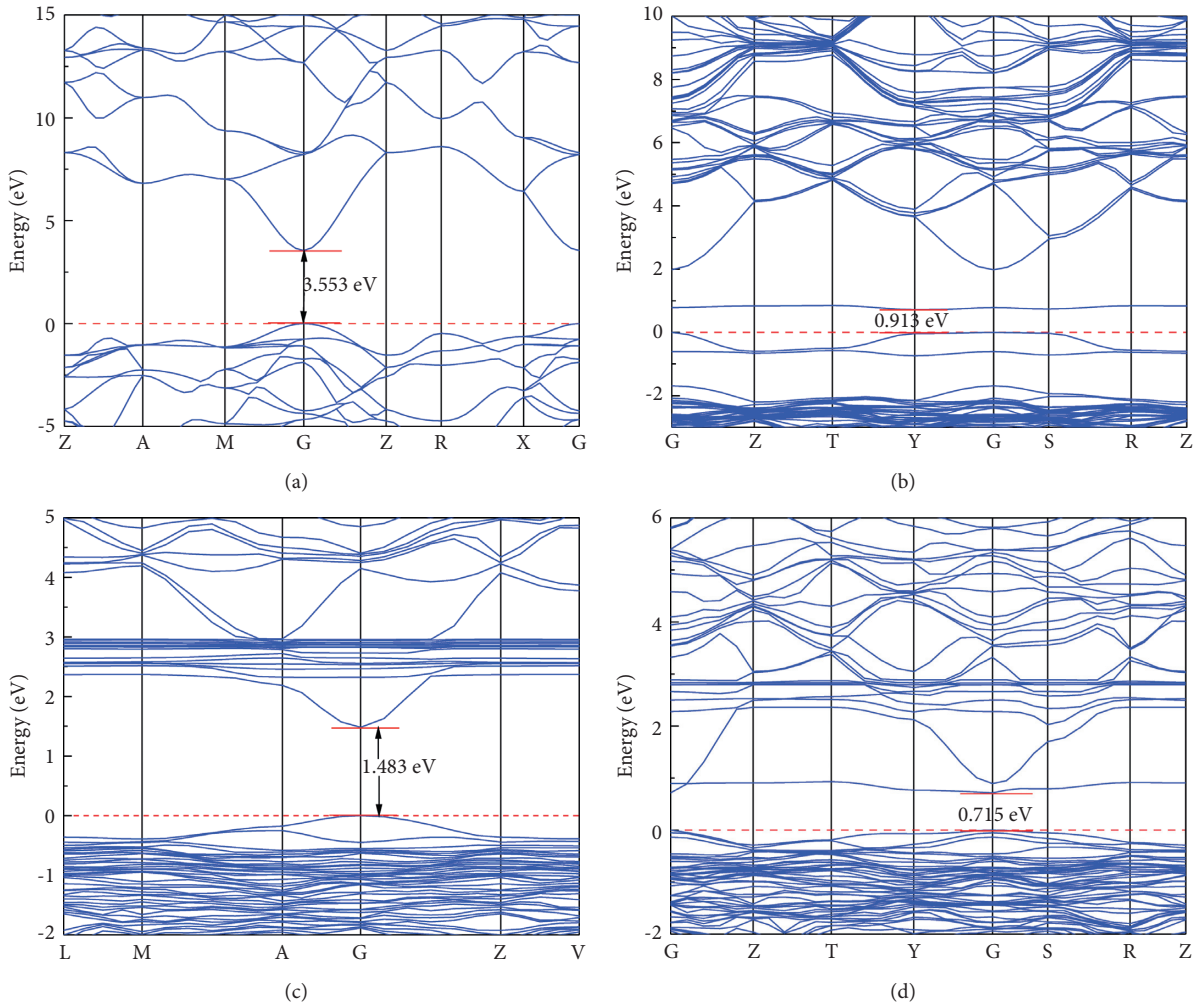

Figure 2: The band structures of: (a) pure SnO_2, (b) C-doped, (c) Ce-doped, and (d) Ce-C codoped.

conduction band shift to *Y* at the high symmetry point of the Brillouin zone. The properties of direct bandgap semiconductors are weakened. Its bandgap is 0.913 eV. Compared with the undoped condition, its bandgap is significantly reduced. There is a very narrow energy level above the Fermi level. The conduction band moves down, and the energy band becomes denser. The energy level of the system has increased significantly. This is because the C atom has 4 electrons in the outermost layer. After the C atom replaces the O atom, it will provide more electrons to the system as a conductive carrier. Therefore, electrons need less energy to transition from the top of the valence band through the Fermi level to the bottom of the conduction band. It enhances the conductivity of SnO_2. Figure 2(c) shows the energy band diagram of Ce-doped SnO_2 with a bandgap of 1.483 eV. Compared with undoped, the bandgap is reduced. The energy levels near the Fermi level increase. Both the valence band and the conduction band move to the Fermi level, so the locality is enhanced. Figure 2(d) is the energy band diagram of Ce-C codoped SnO_2 with a bandgap of 0.715 eV. Compared with Ce and C single doping, it has a smaller bandgap and the densest energy band of the system. Both the valence band and the conduction band move to the Fermi level. More energy levels appear on both sides of the Fermi level. The top of the valence band passes through the Fermi level. Semiconductors appear metallic degeneration. The delocalization of electrons is weakened, and the localization of electrons is enhanced. The energy required for the electronic transition between the valence band and the conduction band is smaller. The conductivity is stronger when the substance is codoped.

3.3. Electronic Density of States. The total and partial densities of states of the initial SnO_2, Ce C single doping, and Ce-C codoping are shown in Figure 3. The total and partial densities of states of the initial SnO_2, Ce C single doping, and Ce-C codoping are shown in Figure 3. Because the region far away from the Fermi level has little effect on the properties of the system, it can be ignored. In this thesis, the density of states in the range of −10~20 eV is selected for analysis. The density of states is mainly analyzed on both sides of the Fermi level. Figure 3(a) is the pure SnO_2 density of states diagram. It can be seen that the densities of states peaks appearing in the valence band (−10~0 eV) are mainly formed by the 5s, 5p, and 2p orbitals of Sn. A spike appears to the left

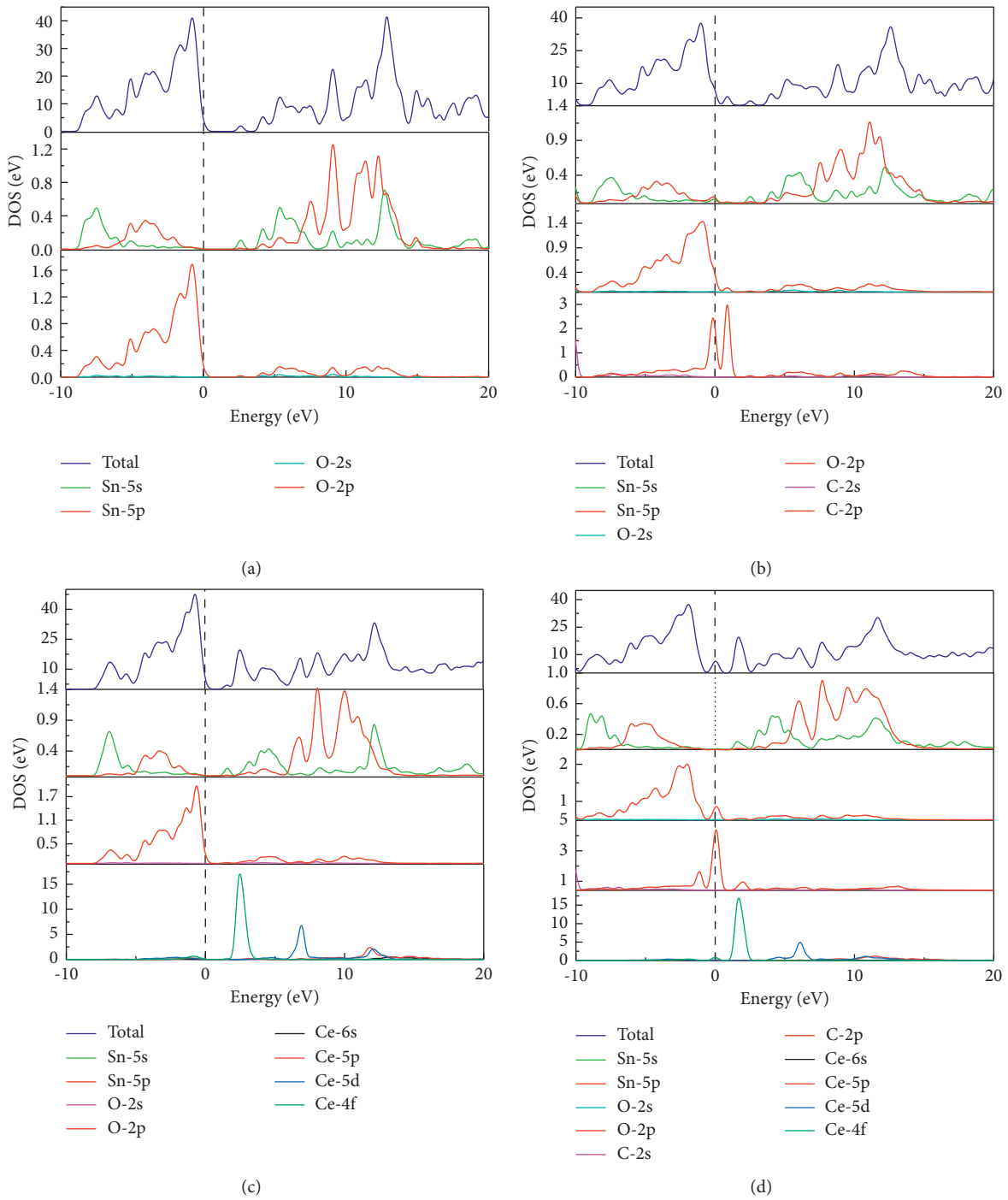

Figure 3: Densities of states: (a) pure SnO_2, (b) C-doped, (c) Ce-doped, and (d) Ce-C codoped.

of the Fermi level. It is mainly contributed by the 2p state of O. The density of states in the conduction band region is mainly contributed by the 5s and 5p hybridization of Sn and the 2p orbital of trace O. There are fewer peaks in the conduction band region near the Fermi level. If no measures are taken, it is difficult for electrons to jump from the top of the valence band into the conduction band. The state of matter is relatively stable at this time.

The densities of states after Ce and C single doping and Ce-C codoping are shown in Figures 3(b)–3(d). Figure 3(b) shows C single-doped SnO_2. In the valence band, Sn's 5s and 5p orbitals and O's 2p orbital peaks have all decreased. The conduction band moves toward the lower energy level as a whole, and a small peak appears at the bottom of the conduction band. It is contributed by the electron density of states peaks appearing on both sides of the Fermi level of the 2p orbital of C. This is the main factor in the reduction of the bandgap. Figure 3(c) shows the density of states of Ce single doping. The density of states near the Fermi level valence band is mainly contributed by the 2p orbital of O. The density

of states near the conduction band of the Fermi level is mainly contributed by the 5s of Sn and the 4f of Ce. The bottom end of the conduction band where the impurity level appears is provided by Ce's 4f state electrons. Figure 3(d) shows the density of states of Ce and C codoped. The two sides of the Fermi level are contributed by the 4f and 5d orbitals of Ce, the 2p orbitals of C, and the 2p orbitals of O. Compared with Ce single-doped SnO_2, the split state density of Ce shifts to a lower energy level as a whole. So more electrons are gathered at the bottom of the conduction band. Codoping will cause more hybrid peaks to form at the bottom of the conduction band. More hybrid peaks appear in the valence band. The electronic localization of the material system is enhanced. A new impurity level is generated at the Fermi level, so the bandgap is further reduced. It also increases the bonding strength between atoms. The increase in metallicity further enhances the conductivity after codoping. This is the same as the result of energy band analysis.

3.4. Charge Density Analysis. Figures 4(a) and 4(b) are the charge density distribution diagrams of intrinsic state SnO_2 and Ce-C codoped, respectively. The comparison shows that the charge density of SnO_2 doped with Ce and C has changed a lot. The electrons are redistributed. When undoped, the electron cloud overlap between Sn and O is small, and the bonding ability is weak. When Ce replaces Sn, the electron cloud density around Ce increases. It overlaps with neighboring O atom electrons, which leads to an increase in the degree of shared electrons and a weakened ability to lose electrons. After the C atom replaces the O atom, the electron cloud appears directional and gathers toward the Ce atom. It forms a strong Ce-C ionic bond. This indicates that when the impurity atoms are introduced, the overlap of the electron shells of the atoms increases, and the electron transfer increases. The number of overlapping populations of charges increases. The degree of Ce-C and Ce-O electronic sharing is strengthened. The electrical conductivity of the system is improved due to the enhancement of the metallicity of the system.

3.5. Mulliken Population Analysis. Tables 2 and 3 are the charge population and bond population of each atom obtained according to the result file of the simulation. All data take the calculated average value.

It can be seen from the charge population in Table 2 that the populations of Sn atoms and O atoms of the initial SnO_2 are 1.86 and −0.93, respectively. It shows that Sn is mainly positively charged due to the loss of electrons, and O is negatively charged mainly due to gaining electrons. Sn and O form an ionic bond. The 2p orbital electron contribution of O is the largest. This is consistent with the density of states analysis. According to the number of charge populations after Ce and C single doping, the 2p orbitals of C and the 5d orbitals of Ce contribute the most electrons. The population number of C is −0.73 because the electrons are negatively charged. The Ce population number of 1.41 is due to the loss of the positive charge of the electron display. Due to the gain and loss of electrons in the material, single doping can enhance conductivity.

When Ce-C codoping, the 2p orbital of C and the 5d orbital of Ce contribute the most electrons. The population of C is −0.66. Compared with single doping −0.73, the number of electrons in C is reduced. The population number of Ce is 1.30. Compared with the population of 1.41 when doped with single doping, it shows that the number of electrons lost in Ce is reduced. Therefore, the ionicity of the Ce-O bond and the Sn-C bond is weakened, and the covalentity is enhanced. The conductivity is further improved than that of single doping. This is in good agreement with the results of energy band and density of states analysis.

From the bond population in Table 3, it can be seen that the overlap population of Sn-O bonds in the intrinsic SnO_2 is 0.38. Sn and O atoms have strong covalentness, and there is a strong charge density overlapping area. In the Ce and C single doping system, hybrid coupling occurs between the doping atoms Ce, C, and Sn atoms. As a result, the number of overlapping populations of Sn-O bonds decreases; the covalency decreases; and the ionicity increases. The electronegativity of Ce and C atoms is smaller than that of Sn and O atoms. Ce-O bond and Sn-C bond are less covalent than Sn-O bond. The interaction is reduced. The population of Sn-C bonds is greater than that of Ce-O bonds, and the covalency is stronger. After Ce-C codoping, the number of free electrons of Ce atoms and C atoms is redistributed. The charge interaction forms a Ce-C covalent bond. The degree of commonality of electrons has also been further improved. Its metallicity is enhanced, and its conductivity is further improved.

3.6. Conductivity. According to the theory of semiconductor physics, the conductivity formula of the SnO_2 doping system can be obtained as follows:

$$\delta_i = n_i q \mu_i, \tag{2}$$

where the n_i represents the electron concentration, q represents the charge constant of electrons, and μ_i represents electron mobility. It can be seen from the formula that the conductivity of a semiconductor is directly proportional to the electron concentration and electron mobility. The electron concentration n_i can be obtained by integrating the density of states. The formula of electron mobility μ_i is as follows:

$$\mu_i \propto \frac{q}{m_e^* \cdot N_i}, \tag{3}$$

where m_e^* represents the effective mass of electrons and N_i represents the doping concentration. Electron mobility is inversely proportional to the effective mass of electrons and doping concentration. The effective electronic mass formula is as follows:

$$m_e^* = \frac{h^2/4\pi^2}{\mathrm{d}^2E/\mathrm{d}k^2}, \tag{4}$$

where h represents Planck's constant, k represents the wave vector, and $\mathrm{d}^2E/\mathrm{d}k^2$ represents the second derivative value at the high symmetry point G in the Brillouin zone of the band structure.

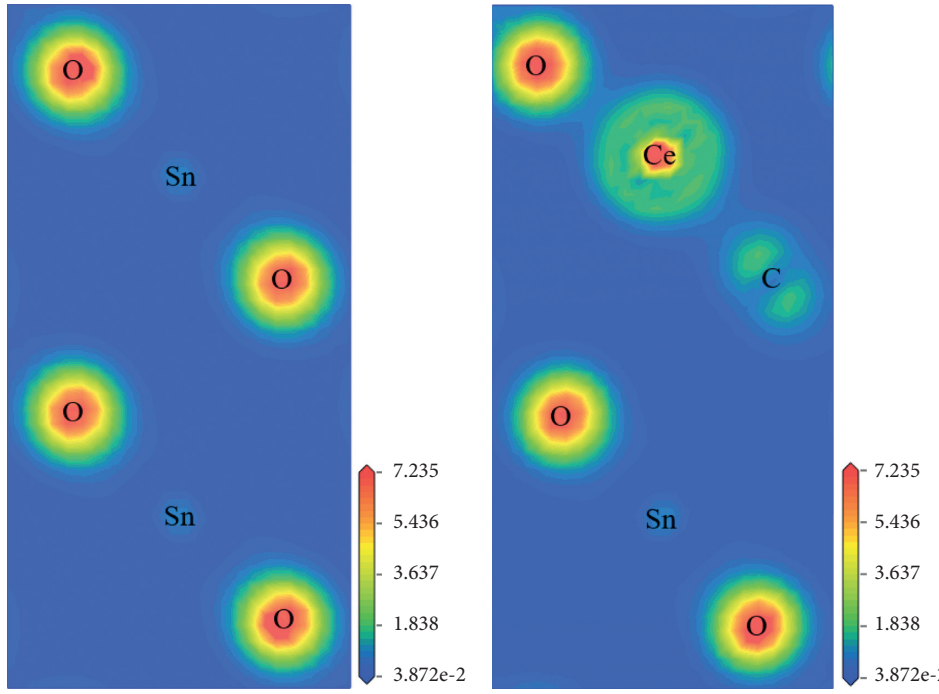

Figure 4: Plots of charge density contour: (a) SnO_2 and (b) Ce-C-SnO_2.

Table 2: Charge populations.

Model	Species	s track	p track	d track	f track	Total population	Charge population
SnO_2	Sn	0.83	1.31	0	—	2.14	1.86
	O	1.85	5.08	0		6.93	−0.93
C-SnO_2	Sn	0.82	1.31	0	—	2.06	1.83
	O	1.85	5.07	0	—	6.93	−0.93
	C	1.66	3.06	0	—	4.73	−0.73
Ce-SnO_2	Sn	0.90	1.28	0	—	2.17	1.82
	O	1.88	5.03	0	—	6.91	−0.91
	Ce	2.26	6.01	1.41	0.92	10.59	1.41
Ce-C-SnO_2	Sn	0.81	1.31	0	—	2.19	1.81
	O	1.85	5.05	0	—	6.91	−0.91
	Ce	2.28	5.90	1.47	1.05	10.70	1.30
	C	1.67	2.99	0	—	4.66	−0.66

Table 3: Bond populations.

Model	SnO_2	C-SnO_2	Ce-SnO_2	Ce-C-SnO_2
Sn-O	0.38	0.34	0.34	0.33
Sn-C	—	0.61	—	—
Ce-O	—	—	0.34	0.33
Ce-C	—	—	—	0.46

Table 4: Related data for conductivity.

Related data	SnO_2	C-SnO_2	Ce-SnO_2	Ce-C-SnO_2
n_i (10^{21} cm^{-3})	7.38	18.65	19.57	20.46
m_e^* (10^{-30} kg)	23.75	14.63	7.21	4.26
δ_i/δ_{SnO2}	1	4.32	9.19	16.29

According to formulas (2)–(4), the conductivity-related parameter values of each doping system can be calculated as shown in Table 4. The conductivity after doping is increased compared with the eigenstate, mainly because the doping concentration increases faster and the effective mass of electrons decreases. When C is doped, it is 4.32 times that of undoped. When Ce is doped, it is 9.19 times that of undoped. When Ce-C is codoped, it is 16.29 times that of undoped. It is similar to the calculated value reported in the related reference [24, 27]. It is concluded that the conductivity of the system is best when codoped.

4. Conclusion

This research is based on the first-principles analysis method of density functional theory. The atom substitution method is used to establish a replacement solid solution model. The

parameters of Ce single doping, C single doping, and Ce-C codoping SnO_2 system are calculated. The parameters include lattice constant, enthalpy change value, energy band, electronic density of state, charge density distribution, and population. The following conclusions can be drawn:

(1) Ce, C single doping, and Ce-C codoping all increase the cell volume and lattice constant. The enthalpy change value shows that the thermal stability of codoping is the best.

(2) Both single doping and codoping reduce the bandgap. They all belong to direct bandgap semiconductors. More energy bands are generated at the top of the valence band and the bottom of the conduction band. The bandgap is the smallest when Ce-C is codoped with SnO_2. The energy band near the Fermi surface is the most, and the energy required for the electronic transition is the least, so the conductivity is the best. When Ce and C are single doped, the 4f orbital electrons of Ce and the 2p orbital electrons of C are the sources of new energy levels near the Fermi level. When Ce-C codoped SnO_2, more energy bands are generated at the bottom of the conduction band and the top of the valence band, which reduces the forbidden band and improves the conductivity.

(3) It can be seen from the charge density and population that the number of free electrons of Ce atoms and C atoms is redistributed after codoping. The charge interaction forms a Ce-C covalent bond. The ionicity of the substance is weakened, and the covalentity is strengthened. The degree of commonality of electrons has also been further improved. The metallicity is enhanced, and the conductivity is further improved. It can also be known from the calculated electrical conductivity of each substance that doping increases the electrical conductivity. When codoped, the conductivity is the largest and the conductivity is the best.

In this paper, doping is used to reduce the bandgap of SnO_2. It provides an idea for improving the conductivity of $AgSnO_2$ contact materials and reducing contact resistance. This research has yet to be studied on its ablation resistance and mechanical properties, in order to improve the performance of the contact in all aspects.

Data Availability

The data used to support the findings of this study are included within the article.

Conflicts of Interest

The authors declare that there are no conflicts of interest.

Acknowledgments

This study was funded by the National Natural Science Foundation (51807069).

References

[1] W. Dong, X. Xie, J. Jia et al., "Theoretical calculation and experimental study on the conductivity and stability of Bi-doped SnO_2 electrode," *Electrochimica Acta*, vol. 132, pp. 307–314, 2014.

[2] Y. Xu, W. Li, D. Wang, X. Wang, A. Yang, and M. Rong, "Research on the gas sensitivity of SnO_2(101) surface to SF_6 decomposition gas based on first principles," *High Voltage Electrical Apparatus*, vol. 55, no. 5, pp. 10–16, 2019.

[3] Z. Chen, S. Zhang, Y. Shao et al., "Relationship between the electric structures calculated by the first principles calculation method and the photoelectrocatalysis degradation of Ir-doped SnO_2 electrodes," *Applied Surface Science*, vol. 422, pp. 891–899, 2017.

[4] W. Ren, X. Wang, M. Zhang, X. Yang, and J. Zou, "Arc erosion behavior of Ag-SnO_2 contact materials with different SnO_2 content," *Rare Metal Materials and Engineering*, vol. 45, no. 8, pp. 2075–2079, 2016.

[5] C. Shao, J. Yu, X. Li, X. Wang, and K. Zhu, "Influence of the Pt nanoscale interlayer on stability and electrical property of Ti/Pt/Sb-SnO_2 electrode: a synergetic experimental and computational study," *Journal of Electroanalytical Chemistry*, vol. 804, pp. 140–147, 2017.

[6] W.-Z. Xiao, H. Luo, J.-Y. Yang, and D. Shuang, "Ferromagnetism in Rh-doped SnO_2 from first-principles calculation," *The European Physical Journal B*, vol. 80, no. 3, pp. 337–341, 2011.

[7] Q. Wang, D. Lu, C. Cui, and M. Xu, "Preparation of doped SnO_2 nanopowders for Cu-based electrical contacts," *Rare Metal Materials and Engineering*, vol. 43, no. 8, pp. 1979–1982, 2014.

[8] G. Ma, L. Zhang, X. Wu et al., "The preparation of Ag/SnO_2 electrical contact materials and their arc-ignition characteristics," *Rare Metal Materials and Engineering*, vol. 49, no. 4, pp. 1312–1324, 2020.

[9] H. Wang, L. Wang, and Z. Wang, "Physical properties and electrical contact characteristics of Ag-SnO_2 contact materials doped with additives of different particle sizes (English)," *Rare Metal Materials and Engineering*, vol. 48, no. 2, pp. 458–462, 2019.

[10] S. Sun, J. Wang, Y. Zhu, G. Zhang, and Z. Bao, "First-principles analysis of the conductivity of La and W co-doped SnO_2," *Materials Review*, vol. 34, no. S1, pp. 48–52, 2020.

[11] Y. Lu, P. Wang, C. Zhang, F. Xianyu, L. Jiang, and G. Zhang, "First-principles analysis of Fe and S co-doped SnO_2 materials," *Acta Physica Sinica*, vol. 61, no. 2, pp. 185–191, 2012.

[12] J. Wang, Y. Zhang, and H. Kang, "Simulation and experimental study on properties of Ag/SnO_2 contact materials doped with different ratios of Ce," *Advances in Materials Science and Engineering*, vol. 2018, Article ID 2524748, 9 pages, 2018.

[13] R. Zhang, Y. Liu, Q. Gao, Fujishige, C. Song, and G. Han, "First-principles study of the electrical properties of rutile phase TiO_2: F and SnO_2: F (English)," *Rare Metal Materials and Engineering*, vol. 41, no. S3, pp. 18–21, 2012.

[14] W. Akbar, I. Elahi, and S. Nazir, "Development of ferromagnetism and formation energetics in 3D TM-doped SnO_2: GGA and GGA + U calculations," *Journal of Magnetism and Magnetic Materials*, vol. 511, pp. 1–8, 2020.

[15] J.-q. Wang, L. Zhou, L. Chen, S. Yu, and Y. Zhu, "Effect of Cu F Co-doping on the properties of $AgSnO_2$ contact," *Materials*, vol. 12, no. 14, pp. 32–39, 2019.

[16] D. Manikandan, A. K. Yadav, S. N. Jha, D. Bhattacharyya, D. W. Boukhvalov, and M. Ramaswamy, "XANES, EXAFS,

EPR, and first-principles modeling on electronic structure and ferromagnetism in Mn doped SnO_2 quantum dots," *Journal of Physical Chemistry C*, vol. 123, pp. 3067–3075, 2019.

[17] H. Kang, J. Wang, and Y. Zhang, "Theoretical analysis of the conductive properties of La and Bi co-doped Ag/SnO_2 contact materials," *Journal of Materials Science and Engineering*, vol. 37, no. 3, pp. 463–468, 2019.

[18] C. Ding, W. Li, J. Liu, L. Wang, Y. Cai, and P. Pan, "First-principles analysis of the electronic structure of Sb and S co-doped SnO_2," *Acta Physica Sinica*, vol. 67, no. 21, pp. 141–147, 2018.

[19] J. Wang, D. Zhou, Y. Li, and P. Wu, "Experimental and first-principle studies of ferromagnetism in Na-doped SnO_2 nanoparticles," *Vacuum*, vol. 141, pp. 62–67, 2017.

[20] Y. Wang, W. Wang, S. Fang, B. Dai, and J. Zhu, "The interface characteristics of TiN(100)/MgO(100) multilayer on oxidized Si(100) substrate via first-principle calculations and experimental investigation," *Molecular Simulation*, vol. 47, no. 7, pp. 36–45, 2021.

[21] R. Santosh and V. Kumar, "The pressure effect on stability, electronic and optical properties of fluorine passivated graphene $(CF)_n$: a first-principle study," *Materials Science & Engineering B*, vol. 269, pp. 1–9, 2021.

[22] J. Xue, X. Zhang, and B. Qiang, "Study on the modification mechanism of $Ti/Sb\text{-}SnO_2$ electrode by La doping: electrochemical analysis," *Rare Metal Materials and Engineering*, vol. 47, no. 8, pp. 2440–2445, 2018.

[23] C. Zhao, J. Wang, Y. Cai, L. Zhou, and Q. Wu, "First-principles analysis of the conductive properties of La-doped $AgSnO_2$ contact materials," *Chinese Journal of Nonferrous Metals*, vol. 27, no. 12, pp. 2552–2559, 2017.

[24] H. Li, J. Wang, S. Sun, Z. Zhang, Y. Liang, and Y. Zhu, "First-principles study on the electrical properties of non-metallic elements NS co-doped SnO_2," *Functional Materials*, vol. 52, no. 2, pp. 2136–2140, 2021.

[25] Y. Du, J. Chen, and F. Jing, "Mechanical properties and electronic structure of different SnO_2 crystal structures," *Acta Physico-Chimica Sinica*, vol. 25, no. 2, pp. 278–284, 2009.

[26] X. Xie, L. Zhong, Z. Liang, C. Fan, and P. Han, "Study on the electronic structure of Ru-doped SnO_2 semiconductor solid solution," *Chinese Journal of Inorganic Chemistry*, vol. 29, no. 12, pp. 2514–2520, 2013.

[27] S. Yu, J. Wang, L. Chen, and L. Zhou, "First-principles study on the electrical properties of dual rare earth elements Ce and Nd co-doped SnO_2," *Rare Metals*, vol. 44, no. 11, pp. 1177–1183, 2020.

[28] C. Peng, B. Lei, X. Tong et al., "First-principles calculations of C-doped SnO_2 at different concentrations," *Journal of Atomic and Molecular Physics*, vol. 35, no. 3, pp. 401–406, 2018.

[29] K. Bakht, T. Mahmood, M. Ahmed, and K. Abid, "Pressure induced electronic and optical properties of rutile SnO_2 by first principle calculations," *Superlattices and Microstructures*, vol. 90, pp. 236–241, 2016.

[30] L. Shan, D. Ba, Q. Cao, X. Hou, and J. Li, "The effect of Ce-Cu co-doping on the optical and electrical properties of SnO_2 thin films," *Acta Metallurgica Sinica*, vol. 50, no. 1, pp. 95–102, 2014.